Journal of Physics D: Applied Physics

PAPER

# Correlation between interface perpendicular magnetic anisotropy and interfacial Dzyaloshinskii–Moriya interactions in Pt/Pd($t_{Pd}$)/Co($t_{Co}$)/Au

To cite this article: D Ourdani *et al* 2022 *J. Phys. D: Appl. Phys.* **55** 485004





IOP Publishing Journal of Physics D: Applied Physics
J. Phys. D: Appl. Phys. **55** (2022) 485004 (8pp) https://doi.org/10.1088/1361-6463/ac9487

# Correlation between interface perpendicular magnetic anisotropy and interfacial Dzyaloshinskii–Moriya interactions in Pt/Pd($t_{Pd}$)/Co($t_{Co}$)/Au

**D Ourdani[1], Y Roussigné[1], S M Chérif[1], M S Gabor[2,*] and M Belmeguenai[1,*]**

[1] Université Sorbonne Paris Nord, LSPM, CNRS, UPR 3407, F-93430 Villetaneuse, France
[2] Center for Superconductivity, Spintronics and Surface Science, Physics and Chemistry Department, Technical University of Cluj-Napoca, Str. Memorandumului No. 28, RO-400114 Cluj-Napoca, Romania

E-mail: mihai.gabor@phys.utcluj.ro and belmeguenai.mohamed@univ-paris13.fr

Received 21 June 2022, revised 14 September 2022
Accepted for publication 23 September 2022
Published 14 October 2022

**Abstract**

The interfacial Dzyaloshinskii–Moriya interaction (iDMI) and perpendicular magnetic anisotropy (PMA) can be manipulated via interface engineering. Their strength determines the generation and the size of skyrmions, and the correlation between the iDMI and PMA allows them to be controlled simultaneously, thus choosing the material parameters for which skyrmions can be formed. This opens up the possibility of synthesizing suitable magnetic multilayers that are needed for low-power high-density memory and in logic applications. Vibrating sample magnetometry (VSM), Brillouin light scattering (BLS), and microstrip ferromagnetic resonance (MS-FMR) were used to investigate the correlation between the iDMI and the interface PMA. For this, Pt/Pd($t_{Pd}$)Co($t_{Co}$)/Au thin film structures with $0 \leqslant t_{Pd} \leqslant 1.2$ nm and 1.2 nm $\leqslant t_{Co} \leqslant 3$ nm were grown by combined sputtering and e-beam evaporation on $Si/SiO_2$ substrates. VSM measurements revealed a negligible magnetic dead layer and a Pd thickness-independent magnetization at saturation of around 1200 emu cm$^{-3}$. MS-FMR and BLS allowed us to conclue that PMA results from weak volume and interfacial contributions induced by Pd/Co or Pt/Co and Co/Au interfaces. The interface anisotropy constants are found to be 0.65 mJ m$^{-2}$ and 0.85 mJ m$^{-2}$ for Pd/Co and for Pt/Co interfaces, respectively. The Pd thickness-dependence of surface iDMI ($D_s$) and PMA ($K_s$) constants follow an exponential decay with a characteristic thickness higher for PMA than the iDMI. The slower decrease of $K_s$ vs Pd thickness suggests a shorter range of the iDMI with respect to PMA and points out a strongly localized origin for the iDMI. This difference between the iDMI and PMA is most likely responsible for the nonlinear correlation between PMA and iDMI constants. The investigation of the Co thickness-dependence of the iDMI and PMA in Pd/Co/MgO/Ta systems allows us to conclude a zero iDMI constant of Co/Au and to determine the iDMI constants of Pd/Co and Co/MgO, estimated to be $D_s^{Pd/Co} = -0.096$ pJ m$^{-1}$ and $D_s^{Co/MgO} = -0.15$ pJ m$^{-1}$, respectively. The criterion of skyrmions stability, applied for our samples, revealed the possibility of the existence of stable skyrmions in some samples.

Keywords: interface effects, perpendicular magnetic anisotropy, ferromagnetic resonance, Brillouin light scattering, interfacial Dzyaloshinskii–Moriya interaction

(Some figures may appear in colour only in the online journal)

* Authors to whom any correspondence should be addressed.

 

## 1. Introduction

The ever-growing need for higher data-processing speeds and larger data-storage capacities has pushed us to seek to create more energy-efficient and faster electronics. In these circumstances, spintronics devices, expected to be faster, denser, and with reduced power consumption, are a promising alternative to complementary metal oxide semiconductor (CMOS) devices [1]. The main technological sector where spintronics is expected to make a big impact, especially after the demonstration of current-induced spin–orbit torques [1, 2], is memory domain [3]. In this domain, topological spin structures such as chiral domain walls and, more specifically, skyrmions [4, 5] are promising information carriers in devices with low power consumption and/or high processing speeds or as q-bits for quantum-information applications [6]. Indeed, skyrmions are expected to be used in the so-called racetrack memory [7]. Their main advantage over domain walls is their potentially very small, nanometer-scale sizes, which could provide denser memory bits integration and a drastically enhanced velocity under small electrical currents.

The crucial ingredients needed for stabilizing these exotic spin chiral textures (skyrmions) is the interfacial Dzyaloshinskii–Moriya interaction (iDMI) and other interactions such as symmetric exchange and effective anisotropy, i.e. the difference between magnetocrystalline and shape anisotropies. The iDMI is a spin–orbit coupling (SOC)-related antisymmetric exchange interaction between neighboring spins, and materials with perpendicular magnetic anisotropy (PMA) are very well suited for these spintronic applications. Indeed, it has been confirmed experimentally that PMA materials increase the thermal stability of devices and can drastically decrease the critical current density of current-induced domain wall motion in magnetic metal nanowires [8, 9]. The strength of the iDMI and PMA, which can be manipulated via interface engineering, determines the generation and the size of skyrmions [10]. Therefore, investigation of the correlation between the iDMI and the PMA plays a key role in the most important spintronic applications, particularly those related to memory and storage. It allows the choosing of the iDMI and the PMA constant values and finding out the material parameters for which skyrmions can be formed.

The correlation between the iDMI and interface PMA could be investigated by identifying the variation of the surface PMA constant ($K_s$) versus that of the iDMI ($D_s$). This can be achieved by changing the ferromagnetic thickness ($t_{FM}$) in typical stacks of heavy metal (HM)/feromagnetic layer (FM)/normalmaterial (NM) incorporating various HMs and capped by a given NM. However, since only a few HMs such as Pt, Ta, Ir, and W induce iDMI, which is moreover markedly weak and with contradictory reported values of $D_s$ for nominally the same system (especially those based on Ta, Ir, and W), other methods should be used. The other method for this correlation investigation is to vary the thickness of the HM layer [11]. Systems based on the insertion of an ultrathin metallic or nonmetallic interlayer (dusting layer) of variable thickness, at the interface the between FM layer and Pt as the HM [12], have also been used for such investigation. Here, Pt is used as the HM since it is known to be the HM with the strongest iDMI. The authors have observed a linear dependence between iDMI and PMA constants and have concluded they are strongly correlated as interface effects that have a SOC-related physical origin [11, 12]. Other authors such as Zhu *et al* [13] have used composition variation in $Au_{1-x}Pt_x$/Co [10] or $Pd_{1-x}Pt_x$ [14] interfaces to significantly tune the iDMI and PMA. Linear [14] or nonlinear [13] dependencies between the effective iDMI and the effective PMA (a sum of the bottom and top interfacial contributions) have been observed. Moreover, Kim *et al* [15] investigated the correlation between the iDMI and the interfacial PMA in Pt/Co/MgO stacks with varying the annealing temperatures and observed a nonlinear correlation by considering the individual contribution of the interfacial magnetic energies at each interface.

In the abovementioned investigations, the thickness of the FM layer is usually fixed, and, therefore, the correlation is investigated by considering PMA and iDMI effective constants, which are FM layer thickness-dependent. Analysis of the correlation between the interfacial PMA and the iDMI should involve the variation of the thickness of the FM layer. Thus, here we consider samples with a Pt/Pd($t_{Pd}$)/Co($t_{Co}$)/Au structure with variable Pd and Co thicknesses ($t_{Pd}$ and $t_{Co}$, respectively). The Pd layer was inserted at the interface between the Pt and Co layers to vary the interfacial SOC perceived by the Co layer. Brillouin light scattering (BLS) coupled to vibrating sample magnetometry (VSM) and FMR experimental techniques are used to precisely characterize the interfacial PMA and the iDMI, and their correlations are studied.

## 2. Samples and experimental techniques

One of the most important difficulties in preparing samples with variable thicknesses is to ensure that all deposition parameters remain precisely the same during growth. Thus, to reduce the variability of the deposition parameters, the Pt/Pd($t_{Pd}$)/Co($t_{Co}$)/Au samples were grown in the same run by employing a double wedge procedure. For this, by using magnetron sputtering, a Ta(2.5)/Pt(1) by-layer was deposited on a $Si/SiO_2$ substrate (the number in parenthesis represents the thickness of the layer in nm). After deposition, the sample was immediately transferred in an ultra-high vacuum e-beam evaporation system and annealed at 125 °C for 1 h in a vacuum higher than $2 \times 10^{-10}$ Torr to remove any water than might have condensed on the sample surface during transfer. After cooling the sample down to 50 °C, a Pt(4) layer was deposited at a rate of 0.01 nm $s^{-1}$. Next, a Pd wedge was grown on the Pt layer using a mobile shutter placed in front of the sample holder. The speed and position of the shutter were controlled to create two regions on the sample: one in which no Pd was deposited and one in which a Pd wedge between 0 and 1.2 nm was grown. Next, the sample holder was rotated in-plane by 90°, and by employing the mobile shutter, a Co wedge between 1.0 and 3.2 nm was grown on top of the Pt/Pd. Finally, the samples were capped with an Au(3) layer. Before performing the measurements, the sample was diced to obtain

$5 \times 5$ samples each with a lateral size of 4 mm. For each sample, the thickness $t_{Co}$ or $t_{Pd}$ of the Co or Pd is the average thickness calculated over the sample surface, except for the samples with $t_{Pd} = 0$ for which no Pd was deposited.

For each sample with a given Pd thickness, the hysteresis loops were measured under an in-plane applied magnetic field using VSM. The saturation magnetic moment per unit area ($M_s \times t_{Co}$) was then calculated versus the Co layer thicknesses. The linear fit of these data gives straightforwardly the magnetization at saturation $M_s$ and the thickness of the magnetic dead layer ($t_d$) from the slope and the horizontal axis intercept. Microstrip line ferromagnetic resonance (MS-FMR) [16] was used to measure the in-plane field-dependence of the uniform precession mode frequency and then deduce the effective magnetization ($4\pi M_{eff}$) of samples with the thicker Co layer ($t_{Co} > 1.6$ nm). BLS [17], under an in-plane applied magnetic field, was used in Damon-Eshbach configuration to investigate the iDMI and PMA. For this, the recorded spectra are fitted with a Lorentzian function to obtain Stokes (S) and anti-Stokes (aS) line frequencies. For PMA, the field dependence of the mean frequency ($F = (F_S + F_{aS})/2$), at a fixed spin wave vector of 8.08 $\mu m^{-1}$ (incident angle of 20°), was used, respectively. The variation of the frequency mismatch between Stokes and anti-Stokes lines ($\Delta F = F_S - F_{aS}$) allowed the iDMI strength to be characterized. All the measurements presented below were carried out at room temperature.

## 3. Results and discussion

Figure 1(a) shows the thickness-dependence of the areal magnetic moment at saturation ($M_s \times t_{Co}$) for three sets of Pt/Pd($t_{Pd}$)/Co/Au samples with different $t_{Pd}$. The magnetization at saturation and the magnetic dead layer thickness obtained from the linear fits of data from figure 1(a) are shown in figure 1(b). Although a slight increase of $M_s$ with the increasing $t_{Pd}$ might be argued from figure 1(a), the change of $M_s$ over the whole Pd thickness range remains within the error bars. Thus, an average $M_s$ value around 1200 emu $cm^{-3}$ is used for all samples. This value is in good agreement with the reported one for Pt/Co/Cu [18] but it is lower than those reported for bulk Co: 1422 emu $cm^{-3}$ for hcp Co and 1450 emu $cm^{-3}$ for fcc Co [19]. This reduction in $M_s$ could be attributed to the fact that the thin Co layers accommodate a substantial proportion of atoms at the interfaces [20]. It is worth noting that the negligible magnetic dead layer for all the samples is compatible with Co–Au immiscibility [20] and the zero-magnetic dead layer of the Pt/Co interface reported by Bandiera *et al* [21]. Therefore, for simplicity, all the measurements presented below are analyzed by considering $M_s = 1200$ emu $cm^{-3}$ and a zero magnetic dead layer to deduce the PMA and iDMI parameters.

The PMA can be determined from the measurement of the field dependence of spin waves frequency through the investigation of the FM thickness-dependence of the effective magnetization ($4\pi M_{eff} = 4\pi M_s - 2K_{eff}/M_s$, where $K_{eff}$ is the PMA effective constant). For this, the MS-FMR technique was systematically used for all samples except for those where the MS-FMR signal was too weak, even undetectable, where the use of the BLS proved to be inevitable. The use of MS-FMR is thus preferable because of its faster acquisition time compared to BLS, which makes it possible to study more samples. Figure 2(a) shows the typical field dependences of the spin wave frequency for Pd-free samples with various Co thicknesses, where the BLS measurements were carried out at a fixed spin wave vector of $k_{sw} = 8.04$ $\mu m^{-1}$. These measurements were then fitted using equation (1):

$$F = \frac{\gamma}{2\pi}\sqrt{\left[H + Jk_{sw}^2 + P\left(k_{sw}t_{Co}\right)4\pi M_s\right]\left[H + Jk_{sw}^2 - P\left(k_{sw}t_{Co}\right)4\pi M_s + 4\pi M_{eff}\right]}. \quad (1)$$

where $H$ is the in-plane applied field, $J = \frac{2A_{ex}}{M_s}$ with $A_{ex}$ is the exchange stiffness constant of Co, $\gamma/(2\pi) = 31 \pm 0.5$ GHz $T^{-1}$ is the gyromagnetic ratio, and $P(k_{sw}t_{eff})$ is defined in [22]. Note that, for BLS, the experimental data are fitted considering $k_{sw} = 0$ $\mu m^{-1}$ in equation (1), since MS-FMR allows for uniform precession mode investigation.

The obtained values of $4\pi M_{eff}$ are shown in figure 2(b) versus $t_{Co}$. For all Pd thicknesses, $M_{eff}$ varies linearly versus the inverse thickness of Co, suggesting the existence of an interfacial contribution to PMA. Therefore, $K_{eff}$ can be described by the phenomenological relationship $K_{eff} = K_v + \frac{K_s}{t_{Co}}$. This allows for the separation of the perpendicular uniaxial surface ($K_s$) and volume anisotropy ($K_v$) constants from the slope and the intercept with the vertical axis of the linear fit of the thickness-dependence of $4\pi M_{eff}$, respectively. The thickness-dependence of these constants will be detailed later together with the thickness behavior of the iDMI constant.

BLS is a powerful method to measure the iDMI constant from the investigation of the $k_{sw}$-dependence of the frequency mismatch $\Delta F$. Usually, spin-wave investigation by BLS, a crossed analyzer, is used to remove the surface phonon Stokes and anti-Stokes lines and therefore, only magnons are present in the BLS spectra. However, the frequency zero position can be shifted if the sample and the reference beams (in Tandem Fabry–Perot set-up) are slightly misaligned, inducing an error in the determination of the iDMI constant, especially for systems with a very weak iDMI. Therefore, the zero frequency position should be checked for each sample and for each measurement involving $k_{sw}$ variation: the positions of the bulk phonon Stokes and anti-Stokes lines should be the same if the zero frequency is well settled. If not, the set-up configuration should be changed in order to recover the same positions for these lines. The acoustic waves can thus be used, if the crossed analyzer is removed, to check the zero frequency

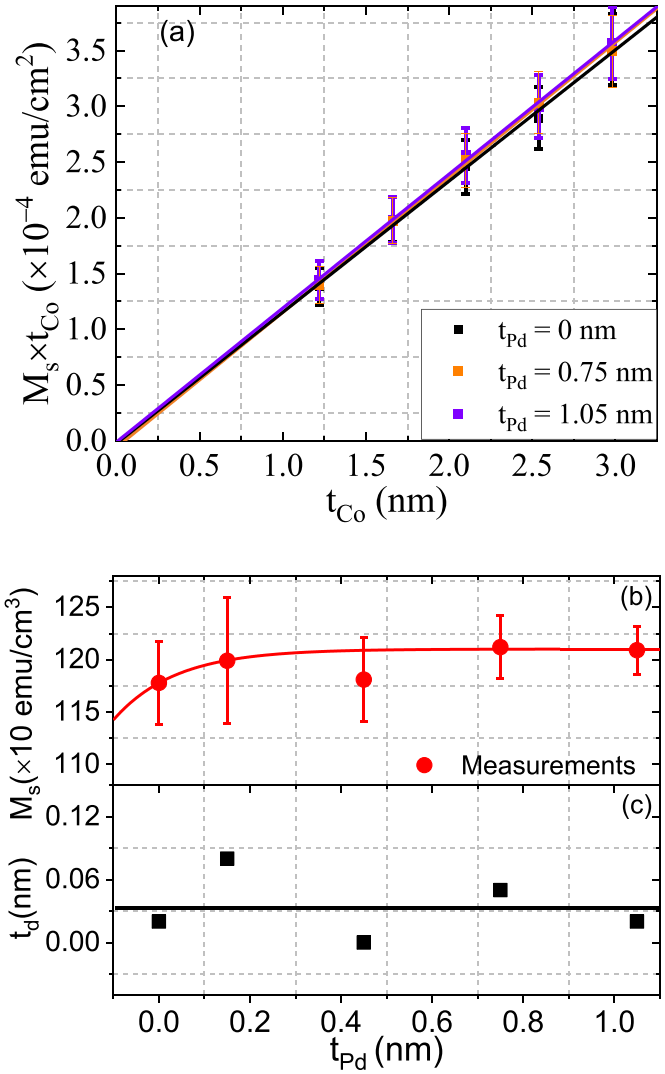


**Figure 1.** (a) Saturation magnetic moment per unit area versus Co thickness ($t_{Co}$) in a Pt/Pd/Co/Au system with various Pd thicknesses ($t_{Pd}$). Symbols refer to the VSM measurements and solid lines are linear fits. Variations of the (b) magnetization at saturation ($M_s$) and (c) magnetic dead layer thickness, deduced from the linear fits of data in (a), versus the Pd thickness. Symbols refer to the experimental data and solid lines are used as guides for the eye.

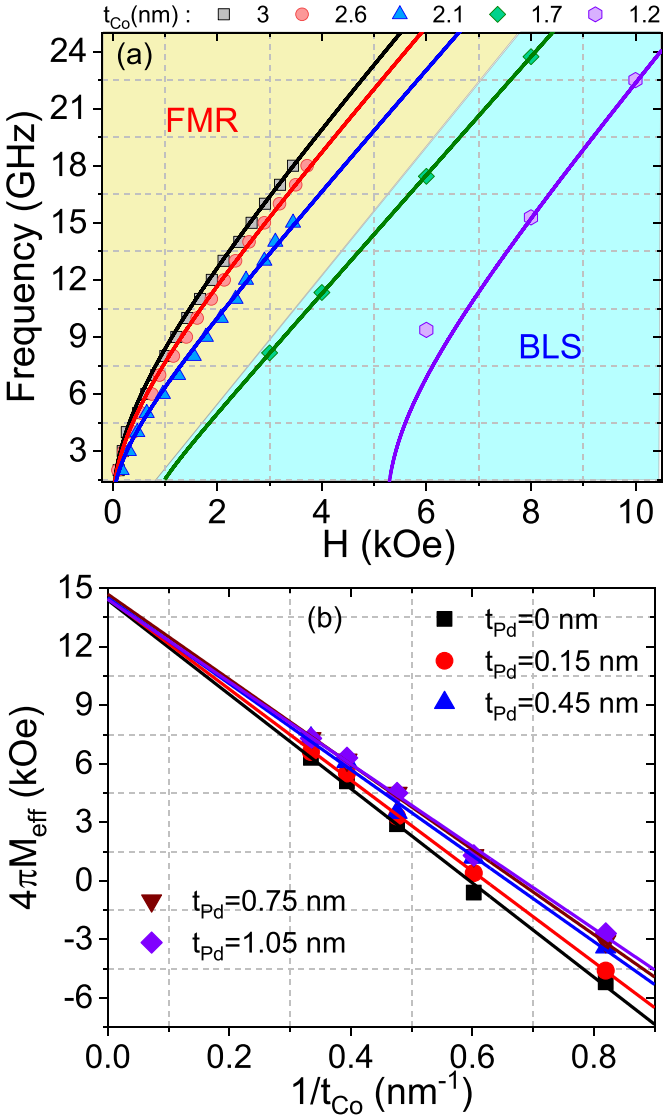


**Figure 2.** Variations of the uniform precession mode frequency (measured by MS-FMR) and the mean frequency ($F = (F_S + F_{aS})/2$), determined from the fit of the recorded BLS spectra at a fixed spin wave vector of 8.08 $\mu$m$^{-1}$ (incident angle of 20°), versus the in-plane applied magnetic field for the Pt/Co/Au sample ($t_{Pd} = 0$ nm). Symbols refer to experimental data and solid lines are fits using equation (1) with $k_{sw} = 0$ or 8.08 $\mu$m$^{-1}$ for MS-FMR or BLS measurements, respectively. (b) Effective magnetization ($4\pi M_{eff}$) versus the inverse of the Co thickness for a Pt/Pd/Co/Au system with various Pd thicknesses ($t_{Pd}$). $4\pi M_{eff}$ values have been extracted from the fit of similar measurements to that in (a). Symbols refer to experimental data while solid lines are linear fits.

setting and proceed to frequency correction for a precise measurement of the iDMI constant. However, the magnetic field should be carefully chosen so that the positions of magnons and phonons are sufficiently far apart to avoid any coupling that interferes with the precise determination of the frequencies of the different lines. Another efficient procedure, consisting of measuring the frequency shift at each $k_{sw}$ for both positive and negative applied fields, could be used to overcome the incorrect adjustment of the zero frequency. However, this method could be time-consuming, in particular when a large number of samples are measured.

Due to the large number of investigated samples in this paper, we limited the determination of the iDMI effective constant ($D_{eff}$) to frequency mismatch $\Delta F$ measurements at maximal $k_{sw} = 20.45$ $\mu$m$^{-1}$ (corresponding to an angle of incidence of 60°) without a crossed analyzer. Figure 3(a) shows the typical BLS spectra for two Pd-free samples with two different Co thicknesses where both phonon (at a lower frequency and which are field-independent) and magnon (at higher frequency) Stokes and anti-Stokes lines are observable. While the frequency mismatch between magnon lines ($\Delta F_{mag}$) is physical and results from the iDMI, the frequency difference between Stokes and anti-Stokes phonon lines ($\Delta F_{ph}$) traduces the incorrect adjustment of the zero frequency and should be used for frequency correction. It is worth mentioning that this

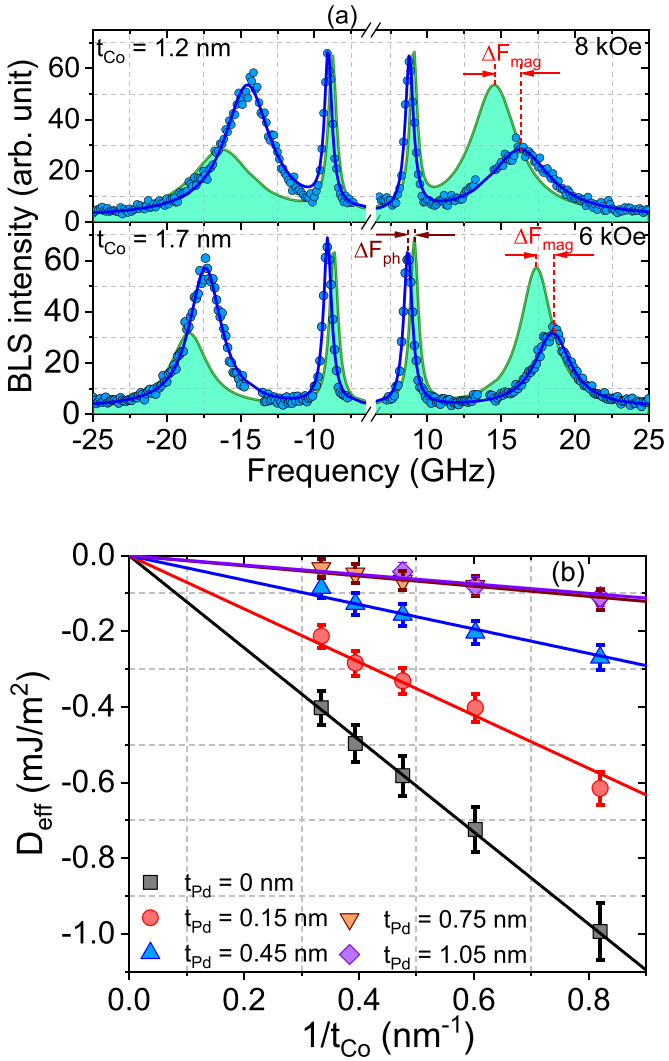


**Figure 3.** (a) BLS spectra measured for two different Co thicknesses of Pt/Co/Au samples ($t_{Pd} = 0$ nm) at different in-plane applied magnetic field values and at a characteristic $k_{sw} = 20.45\ \mu m^{-1}$. Symbols refer to experimental data and solid lines are Lorentzian fits. Fits corresponding to negative applied fields (green lines) are presented for clarity and direct comparison of Stokes and anti-Stokes frequencies. (b) Variation of the effective iDMI constants ($D_{eff}$) versus the Co thickness of the Pt/Pd/Co/Au system with various Pd thicknesses. Solid lines refer to the linear fit and symbols are experimental data.

nonzero frequency difference between phonon lines could lead to an incorrect iDMI value and sign, especially in the case of samples with a very weak iDMI. Therefore, the real value of the frequency mismatch resulting from the iDMI is given by $\Delta F = \Delta F_{mag} - \Delta F_{ph}$. This procedure is used for each sample and the effective iDMI constant ($D_{eff}$) was determined using equation (2):

$$\Delta F = D_{eff}\frac{2\gamma}{\pi M_s}k_{sw} = D_s\frac{2\gamma}{\pi M_s t_{Co}}k_{sw}. \quad (2)$$

where $D_{eff} = D_s/t_{Co}$ and $D_s$ is the iDMI surface constant, characterizing the iDMI strength and $k_{sw} = 20.45\ \mu m^{-1}$.

The variation of $D_{eff}$ versus $1/t_{Co}$ for Pt/Pd($t_{Pd}$)/Co($t_{Co}$)/Au, shown in figure 3(b), reveals a linear behavior allowing us to determine $D_s$ for each $t_{Pd}$. Figure 4(a) shows the Pt thickness-dependence of the surface PMA ($K_s$) and the iDMI ($D_s$) constants, where an exponential decrease (in absolute value) can be distinguished. Notably, we observe a weak amplitude variation of $K_s$ compared *to* $D_s$ over the Pd thickness range, suggesting a comparable contribution of the PMA of Pt/Co and Pd/Co interfaces but almost zero contribution to the total iDMI of the Pd/Co interface. Furthermore, a Pd dusting layer of a single or two atomic planes screens the Pt and efficiently suppresses its contribution to the total iDMI.

For quantitative analysis of the experimental data of figure 4(a), the $t_{Pd}$ dependences of $K_s$ and $D_s$ have been phenomenologically fitted with the exponential function of equation (3). This allows us to quantitatively estimate the characteristic saturation (decay) thickness ($\lambda$: characteristic length associated with the full emergence of PMA and the iDMI), the extent of the PMA or iDMI strength over the $t_{Pd}$, and $K_s$ or $D_s$ values for the Pd/Co/Au system, characterized by $A_1$ and $A_0$, respectively. Note that $K_s$ and $D_s$ of Pt/Co/Au are given by $A_0 + A_1$.

$$y = A_0 + A_1 e^{-\frac{t_{Pd}}{\lambda}}. \quad (3)$$

The exponential fit leads to $K_s = (1.24 \pm 0.04)$ mJ m$^{-2}$ and $(1.44 \pm 0.07)$ mJ m$^{-2}$ for Pd/Co/Au and Pt/Co/Au, respectively. These high values of $K_s$ suggest that both interfaces with Co contribute to the PMA. Therefore, we assumed $K_s = 0.59$ mJ m$^{-2}$ for Co/Au [23] and we obtained the values of $K_s = 0.65$ mJ m$^{-2}$ for the Pd/Co interface and $K_s = 0.85$ mJ m$^{-2}$ for the Pt/Co interface. This $K_s$ value for the Pt/Co interface is in good agreement with the reported values in the literature, found to be in the range 0.6–1.4 mJ m$^{-2}$ [24]. Moreover, the volume anisotropy constant, shown in the inset of figure 4(b), did not show a significant dependence with $t_{Pd}$ (except for $t_{Pd} = 0.75$ nm). Its average value of $3.54 \times 10^{-4}$ J m$^{-3}$ is significantly lower than the bulk magnetocrystalline anisotropy of the hexagonal Co ($K_v = 5.1 \times 10^5$ J m$^{-3}$) [25] and agrees with the literature values for fcc Co [26].

For the iDMI, the obtained values from fits are $D_s = (-0.096 \pm 0.03)$ pJ m$^{-1}$ and $(-1.2 \pm 0.08)$ pJ m$^{-1}$ for Pd/Co/Au and Pt/Co/Au (which is in good agreement with the reported value in the literature [27]). These values suggest a negligible iDMI of the Pd/Co and Co/Au interfaces despite the fact that both of them are HMs. This again raises questions about the microscopic physical origin of the iDMI, although the electronic mechanisms involved in its generation are to be unveiled by theoretical works. Furthermore, the obtained values of $\lambda$ ($\lambda = 0.23$ nm for $D_s$ and $\lambda = 0.58$ nm for $K_s$) reveal a slower decrease of $K_s$, suggesting a shorter range of the iDMI with respect to PMA. This suggests that the iDMI is generated within the two first atomic planes away from the interface, in agreement with first-principles calculations, which point out a strongly localized origin for the iDMI [28–30]. Therefore, the short-range and the interfacial nature of the iDMI open up the possibility to synthesize dense magnetic multilayers using ultrathin layers, allowing for a strong iDMI (in particular in

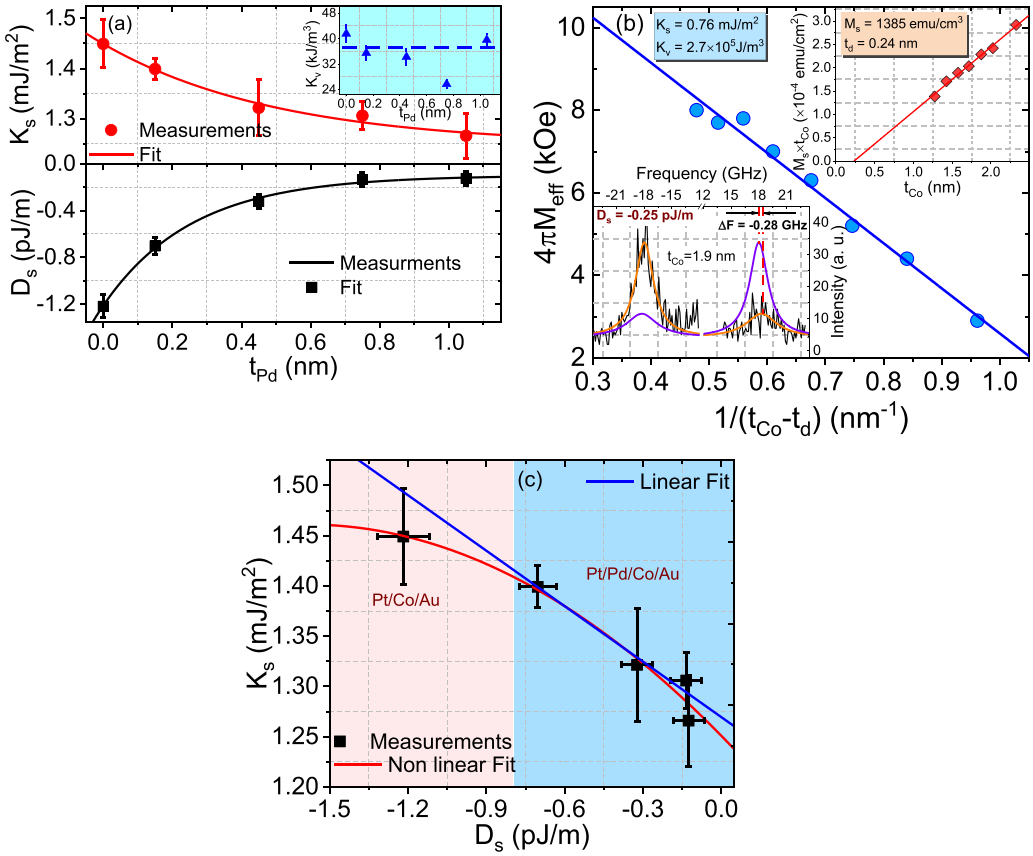


**Figure 4.** (a) Variations of the perpendicular interface anisotropy constant ($K_s$) and the iDMI surface constant ($D_s$) as a function of the Pd dusting layer thickness for the Pt/Pd/Co/Au system with variable Co thicknesses. Symbols refer to experimental data and solid lines are fits with an exponential decay function (equation (3)). (b) Effective magnetization ($4\pi M_{eff}$) versus the inverse of the Co film thickness for the Pt/Pd/Co/MgO system grown on $Al_2O_3$ substrates. Symbols refer to experimental data while solid lines are linear fits. The insets show the corresponding saturation magnetic moment per unit area versus the Co thickness, allowing us to deduce $M_s$ and the magnetic dead layer thickness, and BLS spectra for 1.9 nm-thick Co measured at 6 kOe in-plane applied magnetic field and $k_{sw} = 20.45\ \mu m^{-1}$. (c) Variations of the perpendicular interface magnetic anisotropy constant ($K_s$) as a function of the surface iDMI constant ($D_s$) for the Pt/Pd($t_{Pd}$)/Co($t_{Co}$)/Au system with variable thicknesses. Symbols refer to experimental data and solid lines are linear and second degree polynomial fits. The linear fit is obtained omitting data for Pt/Co/Au samples.

Pt/Co-based systems) even with ultrathin layers due to the absence of distant spin–orbit effects on the iDMI [30].

In order to deepen the analysis, and to have an order of magnitude of the iDMI for each interface as well as the PMA constant of the Pd/Co interface, we grew several samples of Pt(3)/Pd(12)/Co($t_{Co}$)/MgO(1.8)/Ta(2) on a $Al_2O_3$(0001) substrate, where 1.3 nm $\leqslant t_{Co} \leqslant$ 2.4 nm (numbers in parentheses give the nominal thicknesses in nanometers). In order to promote the epitaxial growth on the $Al_2O_3$(0001), the Pt(3) layer was grown at a substrate temperature of 600 °C. The rest of the layers were grown at a temperature of 50 °C. X-ray diffraction experiments (not shown here) indicated epitaxial growth. The VSM measurements of the thickness-dependence of the areal magnetic moment, shown in the inset of figure 4(b), allowed us to deduce $M_s = 1385$ emu cm$^{-3}$ and a magnetic dead layer thickness of 0.24 nm. The enhancement of $M_s$, which is clearly higher than that of samples deposited on Si, proves their superior crystallographic quality. The magnetic dead layer could be associated with a partial oxidation of Co when MgO is deposited on the top. The linear fit of the thickness-dependence of the effective magnetization, shown in figure 4(b), allowed us to obtain $K_s = 0.76$ mJ m$^{-2}$ for Pd/Co/MgO and $K_v = 2.7 \times 10^5$ J m$^{-3}$. This is in line with the obtained $K_s$ value of the Pd/Co interface and confirms that Co grown on $Al_2O_3$ is hexagonal. However, the slightly higher $K_s$ of Pd/Co/MgO compared to that of Pd/Co suggests an additional contribution from the Co/MgO interface.

We also investigated the iDMI constant of Pd/Co/MgO. However, since the measurements are made in backscattering geometry, and due to the transparent nature of the substrate, this degrades the signal-to-noise ratio in particular for the highest values of $k_{sw}$, as shown in the inset of figure 4(b). Moreover, pronounced asymmetry between the amplitudes of Stokes and anti-Stokes lines (see the inset of figure 4(b)), related to the optical properties of Pd, was observed. This constitutes an additional difficulty for iDMI measurements and increases the accumulation time for each spectrum. The iDMI measurements for such system allows us to deduce $D_s = -0.25$ pJ m$^{-1}$. This confirms again the weak iDMI of the Pd/Co interface and suggests a contribution of the Co/MgO interface to the iDMI. Indeed, the highest iDMI values are obtained for Pt/FM

interfaces in combination with oxide top layers [27], suggesting a negative iDMI sign for the FM/MgO interface. Therefore, taking into account the vanishing iDMI of Fe/Au [31], and thus assuming the zero-iDMI of Co/Au, we deduce $D_s^{Pd/Co} = -0.096$ pJ m$^{-1}$ and $D_s^{Co/MgO} = -0.15$ pJ m$^{-1}$. This latter value is in good agreement with the deduced value of Fe/MgO ($D_s^{Fe/MgO} = -0.15$ pJ m$^{-1}$) [31], Co/MgO ($D_s^{Co/MgO} = -0.22$ pJ m$^{-1}$) [32], and CoFeB/MgO ($D_s^{CoFeB/MgO} = -0.17$ pJ m$^{-1}$) [32] from measurements reported in [31, 32]. To the best of our knowledge, this constitutes the first reported measurements for sign and strength of the iDMI in Pd/FM structures.

We will now focus on the correlation between PMA and the iDMI, which can be investigated through the variation of $K_s$ versus $D_s$, as shown in figure 4(c). It reveals a nonlinear dependence of $K_{eff}$ versus $D_{eff}$, which can be explained by different characteristic ranges of the iDMI and interface PMA. Indeed, if the iDMI and PMA are governed by the exponential law given by equation (3), linearity between $K_s$ and $D_s$ is only possible if their $\lambda$ values are the same. To satisfactorily fit the experimental behavior of $K_s$ versus $D_s$, a second-order dependence is necessary. It is worth mentioning that a linear fit of the data can be obtained by neglecting the value for Pt/Co/Au but second-order polynomial fit is more convenient and fits the experimental data better. This is due to the shorter range of the iDMI with respect to the interface PMA. Moreover, in a Pt/Pd/Co/Au system, the iDMI results mainly from the Pt/Co interface modulated by the Pd dusting layer while the PMA is induced by the Pt/Co or Pd/Co and Co/Au interfaces. Therefore, due to the large spin diffusion length of Pd (8.6 nm) [33], the PMA could continue to vary with the Pd dusting layer thickness beyond the single or two atomic planes of Pd needed to efficiently or completely suppress the contribution of Pt to the total iDMI. This could be another reason to explain the range difference between the iDMI and PMA.

We should mention that it is well accepted that electronegativity [34], intermixing [28], proximity magnetism [28], orbital anisotropy, roughness [35], and orbital hybridization [28] affect the iDMI. Due to the similar electronegativity of Pd and Pt (2.2) [13], electronegativity variation with Pd thickness seems unlikely to occur. However, linear correlation between the iDMI and PMA constants was found in $Pd_{1-x}Pt_x$/Co attributed to the linear variations of both the $K_s$ of the $Pd_{1-x}Pt_x$/Co interface and the interfacial SOC as a function of the $Pd_{1-x}Pt_x$ composition [14]. Furthermore, using a composition modulation, no linear correlation between the iDMI and PMA constants is obtained for $Au_{1-x}Pt_x$/Co. This allows us to conclude that the variation of the iDMI at the $Au_{1-x}Pt_x$/Co interface with $x$ cannot be attributed to the change of orbital anisotropy and other mechanisms, such as the interfacial orbital hybridization, play a fundamental role in the iDMI [13]. Therefore, the observed correlation in our systems could result from interfacial SOC besides other contributions such as interfacial orbital hybridization, roughness, and proximity magnetism.

In recent years, skyrmions have attracted a lot of interest as potential candidates for novel spintronics devices. As mentioned above, the iDMI can be used to stabilize that structure.

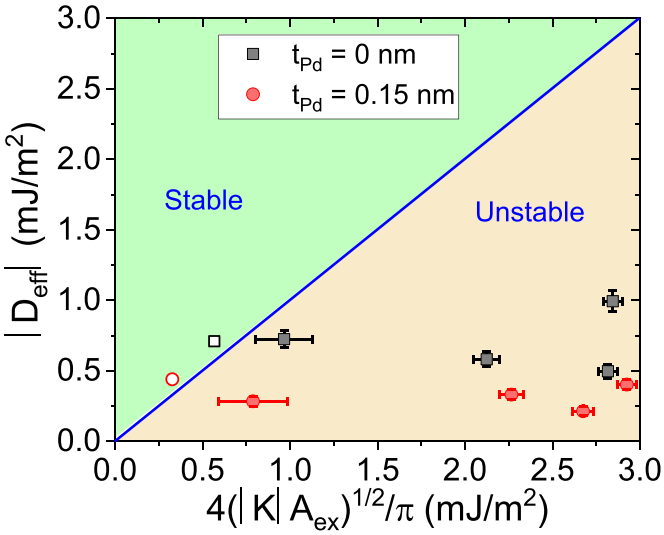


**Figure 5.** Variation of $D_{eff}$ versus $D_c = \frac{4}{\pi}\sqrt{KA_{ex}}$ for Pd-free and 0.15 nm Pd samples with various Co thicknesses, calculated using the obtained experimental magnetic parameters of figures 2(b) and 3(b) and $A_{ex} = 1.6 \times 10^{-11}$ J m$^{-1}$. Open symbols refer to the expected data obtained from extrapolation of the Co thickness dependences of $D_{eff}$ and $4\pi M_{eff}$ of figures 2(b) and 3(b). The solid blue line refers to $D_{eff} = D_c$.

To check whether the reported iDMI values are sufficient to stabilize such spin textures, we calculated the critical value of $D_{eff}$ ($D_c$) above which skyrmions can be stabilized: $D_c = \frac{4}{\pi}\sqrt{KA_{ex}}$ [36], where $K = |2\pi M_{eff}M_s|$ is the effective anisotropy constant and $A_{ex}$ is the exchange stiffness constant. This means that the iDMI energy should be higher than the domain wall energy. In other words, the magnetization should not have a fixed direction to allow the iDMI to rotate it continuously with a given chirality. This implies that the perpendicular effective anisotropy field is very small (ideally zero). As a result, samples with a Co thickness giving an effective magnetization close to zero (see figure 2(b)) are more favorable for hosting skyrmions. Using the obtained experimental magnetic parameters and $A_{ex} = 1.6 \times 10^{-11}$ J m$^{-1}$, the variation of $D_{eff}$ versus $D_c$ is shown in figure 5 for Pd-free and 0.15 nm Pd samples with various Co thicknesses. Figure 5 reveals that only the 1.66 nm thick Co with Pd-free or $t_{Pd} = 0.15$ nm samples (Pt/Co(1.66 nm)/Au and Pt/Pd(0.15 nm)/Co(1.66 nm)/Au) could have stable skyrmions since the stability criterion is almost verified. $D_{eff}$ and $K$ are strongly magnetic film thickness-dependent and could be carefully adjusted so that the stabilization criterion is verified. To achieve this, we used the experimental data of the Co thickness-dependences of $M_{eff}$ and $D_{eff}$ shown in figures 2(b) and 3(b), respectively, to tune the Co thickness. This leads, for example, to Co thicknesses of 1.7 nm and 1.64 nm for Pd-free or $t_{Pd} = 0.15$ nm samples, respectively (data with open symbols in figure 5).

## 4. Conclusion

The correlation between the iDMI and PMA has been investigated in a Pt/Pd($t_{Pd}$)/Co($t_{Co}$)/Au system with variable Co and

Pd thicknesses. VSM measurements, used to determine the magnetization at saturation ($M_s$) and the magnetic dead layer thickness ($t_d$), revealed almost constant $M_s$ and negligible $t_d$. The PMA results from a volume contribution comparable to that of fcc Co besides an interface term that we quantified for each interface. The Pd thickness-dependence of the surface iDMI ($D_s$) and PMA ($K_s$) constants have been phenomenologically fitted to determine the characteristic decay thickness, the extent of PMA, or the iDMI strength over the $t_{Pd}$ and $K_s$ or $D_s$ values for the Pd/Co/Au system. We concluded to slower decrease of $K_s$, suggesting a shorter range of the iDMI with respect to the PMA. This suggests that the iDMI is generated within the first two atomic planes away from the interface, in agreement with first-principles calculations, which point out a strongly localized origin for the iDMI. This short-range of the iDMI opens up the synthesis of dense magnetic multilayers with a strong interfacial iDMI, especially if a Pt/Co interface is used. By investigation of the PMA and iDMI in Pt/Pd/Co($t_{Co}$)/MgO samples grown on $Al_2O_3$, we obtained $K_s$ of Pt/Co and Pd/Co interfaces and deduced $D_s$ values for Co/Au (found to be zero), Pd/Co, and Co/MgO, which were found to be weak and have negative signs. The investigation of the correlation between the iDMI and PMA revealed a nonlinear behavior resulting from the difference in the ranges of their sensitivity to the interface SOC and the strongly localized origin for the iDMI. The criterion for skyrmions stability, applied for our samples, revealed the possibility of the existence of stable skyrmions in some samples.

## Data availability statement

The data generated and/or analyzed during the current study are not publicly available for legal/ethical reasons but are available from the corresponding author on reasonable request.

## Acknowledgments

This work has been supported by the Conseil regional d'Île-de-France (convention 1763) through the DIM NanoK (BIDUL project). M S G acknowledges the financial support for this work from MRID, CNCS/CCCDI—UEFISCDI, through Grant PN-III-P4-ID-PCE-2020-1853-SPINSYNE.

## ORCID iDs

Y Roussigné https://orcid.org/0000-0001-7698-8092
S M Chérif https://orcid.org/0000-0003-4350-9379
M S Gabor https://orcid.org/0000-0003-0888-0762
M Belmeguenai https://orcid.org/0000-0002-2395-1146

## References

[1] Miron I M, Gaudin G, Auffret S, Rodmacq B, Schuhl A, Pizzini S, Vogel J and Gambardella P 2010 *Nat. Mater.* **9** 230
[2] Garello K, Miron I M, Avci C O, Freimuth F, Mokrousov Y, Blügel S, Auffret S, Boulle O, Gaudin G and Gambardella P 2013 *Nat. Nanotechnol.* **8** 587
[3] Barla P, Joshi V K and Bhat S 2021 *J. Comput. Electron.* **20** 805–37
[4] Schmidt L, Hagemeister J, Hsu P-J, Kubetzka A, von Bergmann K and Wiesendanger R 2016 *New J. Phys.* **18** 075007
[5] Sampaio J, Cros V, Rohart S, Thiaville A and Fert A 2013 *Nat. Nanotechnol.* **8** 839
[6] Psaroudaki C and Panagopoulos C 2021 *Phys. Rev. Lett.* **127** 067201
[7] Parkin S S P, Hayashi M and Thomas L 2008 *Science* **320** 190–4
[8] Fukami S, Suzuki T, Ohshima N, Nagahara K and Ishiwata N 2008 *J. Appl. Phys.* **103** 07E718
[9] Koyama T *et al* 2011 *Nat. Mater.* **10** 194
[10] Behera A K, Mishra S S, Mallick S, Singh B B and Bedanta S 2018 *J. Phys. D: Appl. Phys.* **51** 285001
[11] Kim N-H, Han D-S, Jung J, Park K, Swagten H J, Kim J S and You C-Y 2017 *Appl. Phys. Express* **10** 103003
[12] Benguettat-El Mokhtari I, Ourdani D, Roussigné Y, Mos R B, Nasui M, Chérif S M, Stachkevich A, Gabor M S and Belmeguenai M 2020 *J. Phys. D: Appl. Phys.* **53** 505003
[13] Zhu L, Zhu L, Ma X, Li X and Buhrman R A 2020 (arXiv:2007.09817)
[14] Zhu L, Sobotkiewich K, Ma X, Li X, Ralph D C and Buhrman R A 2019 *Adv. Funct. Mater.* **29** 1805822
[15] Kim W-Y, Gweon H K, Lee K-J and You C-Y 2019 *Appl. Phys. Express* **12** 053007
[16] Belmeguenai M, Tuzcuoglu H, Gabor M S, Petrisor T Jr, Tiusan C, Berling D, Zighem F, Chauveau T, Chérif S M and Moch P 2013 *Phys. Rev.* B **87** 184431
[17] Belmeguenai M, Gabor M S, Roussigné Y, Stashkevich A, Chérif S M, Zighem F and Tiusan C 2016 *Phys. Rev.* B **93** 174407
[18] Gweon H K, Yun S J and Lim S H 2018 *Sci. Rep.* **8** 1266
[19] Won Y C and Lim S H 2021 *Sci. Rep.* **11** 10779
[20] Mazalskil P *et al* 2021 *New J. Phys.* **23** 023015
[21] Bandiera S, Sousa R C, Rodmacq B and Dieny B 2011 *IEEE Mag. Lett.* **2** 3000504
[22] Belmeguenai M, Adam J-P, Roussigné Y, Eimer S, Devolder T, Kim J-V, Cherif S M, Stashkevich A and Thiaville A 2015 *Phys. Rev.* B **91** 180405(R)
[23] Cagnon L, Devolder T, Cortes R, Morrone A, Schmidt J E, Chappert C and Allongue P 2001 *Phys. Rev.* B **63** 104419
[24] Dieny B and Chshiev M 2017 *Rev. Mod. Phys.* **89** 025008
[25] Camarero J, de Miguel J J, Miranda R, Raposo V and Hernando A 2001 *Phys. Rev.* B **64** 125406
[26] Guo G Y, Roberts D J and Gehring G A 1999 *Phys. Rev.* B **59** 14466
[27] Kuepferling M, Casiraghi A, Soares G, Durin G, Garcia-Sanchez F, Chen L, Back C H, Marrows C H, Tacchi S and Carlotti G 2022 (arXiv:2009.11830v3)
[28] Yang H, Thiaville A, Rohart S, Fert A and Chshiev M 2015 *Phys. Rev. Lett.* **115** 267210
[29] Jia H, Zimmermann B and Blügel S 2018 *Phys. Rev.* B **98** 144427
[30] Legrand W *et al* 2022 *Phys. Rev. Mater.* **6** 024408
[31] Zhang W *et al* 2019 *Phys. Rev. Appl.* **12** 064031
[32] Ma X, Yu G, Tang C, Li X, He C, Shi J, Wang K L and Xiaoqin L 2017 *Phys. Rev. Lett.* **120** 157204
[33] Shaw J M, Nembach H T and Silva T J 2012 *Phys. Rev.* B **85** 054412
[34] Torrejon J, Kim J, Sinha J, Mitani S, Hayashi M, Yamanouchi M and Ohno H 2014 *Nat. Commun.* **5** 4655
[35] Samardak A S *et al* 2020 *NPG Asia Mater.* **12** 51
[36] Rohart S and Thiaville A 2013 *Phys. Rev.* B **88** 184422